Interplay between sequential and prompt two-proton decay from the first excited state of ^{16}Ne

K. W. Brown, R. J. Charity, L. G. Sobotka, L. V. Grigorenko, T. A. Golubkova, S. Bedoor, W. W. Buhro, Z. Chajecki, J. M. Elson, W. G. Lynch, J. Manfredi, D. G. McNeel, W. Reviol, R. Shane, R. H. Showalter, M. B. Tsang, J. R. Winkelbauer, and A. H. Wuosmaa

Phys. Rev. C **92**, 034329 — Published 30 September 2015

DOI: 10.1103/PhysRevC.92.034329

Interplay between sequential and prompt two-proton decay from the first excited state of ^{16}Ne

K.W. Brown,[1] R.J. Charity,[1,*] L.G. Sobotka,[1] L.V. Grigorenko,[2,3,4] T.A. Golubkova,[5] S. Bedoor,[6,7] W.W. Buhro,[8] Z. Chajecki,[8,†] J.M. Elson,[1] W.G. Lynch,[8] J. Manfredi,[8] D.G. McNeel,[6,7] W. Reviol,[1] R. Shane,[8] R.H. Showalter,[8] M.B. Tsang,[8] J.R. Winkelbauer,[8] and A.H. Wuosmaa[6,7]

[1] *Departments of Chemistry and Physics, Washington University, St. Louis, Missouri 63130, USA*
[2] *Flerov Laboratory of Nuclear Reactions, JINR, RU-141980 Dubna, Russia*
[3] *National Research Nuclear University "MEPhI", Kashirskoye shosse 31, RU-115409 Moscow, Russia*
[4] *National Research Centre "Kurchatov Institute", Kurchatov sq. 1, RU-123182 Moscow, Russia*
[5] *Advanced Educational and Scientific Center, Moscow State University, Kremenchugskaya 11, RU-121357 Moscow, Russia*
[6] *Department of Physics,University of Connecticut, Storrs, CT 06269, USA*
[7] *Department of Physics, Western Michigan University, Kalamazoo, Michigan 49008, USA*
[8] *National Superconducting Cyclotron Laboratory and Department of Physics and Astronomy, Michigan State University, East Lansing, Michigan 48824, USA*

The first-excited, $J^\pi = 2^+$ state of ^{16}Ne at $E^* = 1.69(2)$ MeV is well populated in neutron knockout reactions with a ^{17}Ne beam and the correlations between the momenta of the three final fragments following $2p$ decay were measured. The correlation pattern showed aspects of both sequential and diproton-like decay, which were reproduced in three-body ^{14}O+p+p calculations. These calculations suggest that interference between these processes is responsible for the observed features which can be described in terms of a "tethered decay mechanism". The intrinsic width of this state was constrained to be from 100 to 250 keV. Higher excited states populating the ^{13}N+p+p+p exit channel were found at $E^* = 8.37(10)$ and 10.76(20) MeV.

PACS numbers: 25.10.+s, 23.50.+z, 21.60.Gx, 27.20.+n

I. INTRODUCTION

Two-proton ($2p$) decay is most commonly considered as either of two extreme types: prompt or sequential. In the first case, which is also called "true" $2p$ decay, the two protons are emitted simultaneously in a three-body process. In sequential $2p$ decay, the two protons are emitted in two distinct steps of binary decay. If the intermediate system formed after the first step of single-proton decay is long-lived (narrow), then there will be no interactions between the two protons. Ground-state true $2p$ emitters occur where either no intermediate state is accessible via single-proton emission and/or the width of the intermediate state is wide compared to the single-proton decay energy [1]. For the excited states of such nuclei, these conditions may no longer apply and as the excitation energy increases, and intermediate states becomes fully accessible by single-proton decay, it has generally been assumed that sequential decay will prevail. In this work we investigate such a case and show the transition from prompt to sequential is nontrivial.

Recently we have published first results concerning the $2p$ decay of ^{16}Ne states populated in neutron knockout reactions with a ^{17}Ne beam [2]. In that work, we concentrated on the ground-state of ^{16}Ne which belongs to the class of true two-proton emitters [1, 3] because the ^{15}F $s_{1/2}$ ground state (g.s.) is not fully accessible by single-proton decay as indicated in the decay scheme of Fig. 1. The experimental data used in Ref. [2] has high statistics and excellent resolution allowing us to isolate the effect of the long-range, three-body, Coulomb interactions on the momentum distributions of the decay fragments. This effect was well reproduced by our three-body model thus validating its use with heavier $2p$ decays and allowing one to separate out the finer aspects of the decay dynamics.

Here, we continue our study of the ^{16}Ne continuum and consider the decay of the first excited, $J^\pi = 2^+$ state of ^{16}Ne. From the level scheme in Fig. 1, one expects that the decay of this state is sequential as the ^{15}F $s_{1/2}$ g.s. is fully accessible via one proton decay and the decay energy for this step is large compared to the width of this state. In this case, the decay energy could be efficiently shared between the degrees of freedom (first emitted proton and the motion of ^{15}F), which should provide favorable conditions for penetration. However, both the experimental data and calculations indicate that the real situation is much more complicated.

A similar problem was encountered in our previous studies of the ^{6}Be continuum in Refs. [4, 5]. There we searched for the decay energy E_T at which true $2p$ decay is replaced by the sequential decay mechanism. In contrast to expectations, we found that such a transition *did not take place* in the whole observed energy range ($E_T < 10$ MeV). The decay remained of a complicated three-body nature even if some aspects of the decay cor-

* charity@wustl.edu
† Present Address: Department of Physics, Western Michigan University, Kalamazoo, Michigan 49008, USA

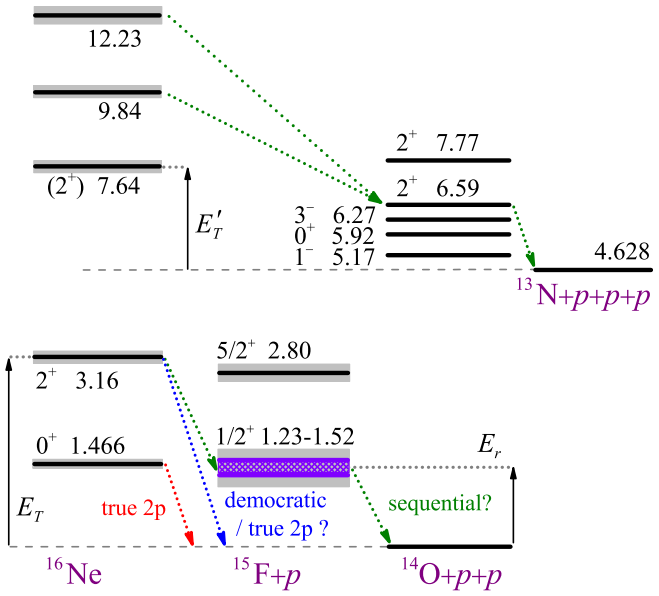

FIG. 1. (Color online) Low-lying levels of ^{16}Ne observed in this work and Ref. [2] and levels important for proton and multi-proton decay to ^{15}F, ^{14}O, and ^{13}N states. The experimental uncertainty of the ^{15}F g.s. energy is indicated by hatching. Note a reduction 1.5 in the scale above the ^{13}N+p+p+p threshold. All level energies are given with respect to the ^{14}O+p+p threshold.

relations resembled the pattern expected for sequential decay. We now find similar results in the decay of the first-excited state of ^{16}Ne.

In ^{16}Ne, the Coulomb interaction is much stronger than in ^{6}Be giving rise to higher Coulomb barriers and thus narrower states. Another difference is that ^{16}Ne belongs to the *s-d* shell and is built on positive-parity single-particle excitations. It is interesting to see if these factors give rise to qualitative differences in the evolution of the decay mechanism with decay energy. This study will help us to predict the behavior for other *s-d* shell 2*p* emitters, for which similar quality data is not available.

Information on higher-lying excited states of ^{16}Ne is very sparse, apart from the observation of another excited state in the ^{14}O+p+p exit channel at $E^* \sim 9.07$ MeV [2, 6, 7] and the possibility of a second 0^+ state at $E^* \sim 2.1$ MeV [8]. At even higher excitation energies, the ^{13}N+p+p+p exit channel opens and from its measured invariant-mass spectrum we find two new excited states.

II. THEORETICAL MODELS

In this work we use two theoretical approaches treating the decaying ^{16}Ne system as an inert ^{14}O core interacting with two protons. One model is semianalytical with a simplified Hamiltonian, and the second is a rigorous three-body cluster model. Three types of information describing the three-body states can be derived theoretically; its resonance energy, its decay width, and the correlations between the momenta of the decay products. The three-body model provides predictions for all of the above quantities while the simplified model can be used to evaluate the width and, in some cases, the correlations can also be described reasonably well.

The correlations between the momenta in three-body decay are defined by a two-dimensional distribution [9]. Typically one axis of this distribution is taken as the energy parameter ε while the other is the angle θ_k between the Jacobi momenta $\mathbf{k}_x$, $\mathbf{k}_y$:

$$\varepsilon = E_x/E_T\,, \qquad c_k = \cos(\theta_k) = (\mathbf{k}_x \cdot \mathbf{k}_y)/(k_x\, k_y)\,,$$
$$\mathbf{k}_x = \frac{A_2\mathbf{k}_1 - A_1\mathbf{k}_2}{A_1 + A_2}\,, \quad \mathbf{k}_y = \frac{A_3(\mathbf{k}_1 + \mathbf{k}_2) - (A_1 + A_2)\mathbf{k}_3}{A_1 + A_2 + A_3}\,,$$
$$E_T = E_x + E_y = \frac{A_1 + A_2}{A_1 A_2}\frac{k_x^2}{2M} + \frac{A_1 + A_2 + A_3}{(A_1 + A_2)A_3}\frac{k_y^2}{2M}, \quad (1)$$

where A_1, A_2, and A_2 are the mass numbers of the three fragments with momenta $\mathbf{k}_1$, $\mathbf{k}_2$, and $\mathbf{k}_3$, respectively and $(A_1 + A_2 + A_3)M$ is the mass of the parent nucleus. With the assignment $k_3 \to k_{^{14}\mathrm{O}}$ ($A_1 = A_2 = 1$ and $A_3 = A_{core}$), the correlations are obtained in the "T" Jacobi system where ε describes the relative energy E_{pp} in the p-p channel. Choosing $k_3 \to k_p$ ($A_2 = A_3 = 1$ and $A_1 = A_{core}$), the correlations are obtained in the "Y" Jacobi system where ε describes the relative energy $E_{\text{core-}p}$ in the ^{14}O-p channel.

A. Simplified decay model

The width and momentum distributions in the "Y" Jacobi system can be estimated within the so-called "direct decay" R-matrix model from Ref. [1] where each proton is assumed to be in a resonant state of the core+p subsystem with resonant energy E_{j_i}. The differential flux for a system of total spin J is given by

$$\frac{dj^{(J)}_{j_1 j_2}(E_T)}{d\varepsilon\, dc_k} = \frac{E_T\,\langle V_3\rangle^2}{2\pi}\, f^{(J)}_{j_1 j_2}(c_k) \times \frac{\Gamma_{j_1}(\varepsilon E_T)}{(\varepsilon E_T - E_{j_1})^2 + \Gamma^2_{j_1}(\varepsilon E_T)/4} \times \frac{\Gamma_{j_2}((1-\varepsilon)E_T)}{((1-\varepsilon)E_T - E_{j_2})^2 + \Gamma^2_{j_2}((1-\varepsilon)E_T)/4}, \quad (2)$$

where j_i is the angular momentum of a core+p_i subsystem. This model can be traced to the simplified Hamiltonian of the three-body system in which the nucleons interact with the core, but not with each other. It approximates the true three-body decay mechanism and also provides a smooth transition to the sequential-decay regime [10, 11]. It is essentially a single-particle approximation treating the decays of configurations $[j_1 j_2]_J$ independently and neglecting interactions between the valence nucleons. The quantity $\Gamma_{j_i}(E)$ is provided by the

standard two-body R-matrix expression for the decay width as function of energy for the core+p_i resonance. The values $\Gamma_{j_i}(E_{j_i})$ correspond to the empirical values of the resonance widths in both core-nucleon subsystems i.

The angular-distribution function $f^{(J)}_{j_1 j_2}(c_k)$ in this model is obtained by coupling the single-particle angular functions with momenta j_1 and j_2 to total momentum J. This function does not always give realistic angular distributions [1]. However for the [sd] configurations, dominating in the decay of the ^{16}Ne $J^\pi = 2^+$ state, $f^{(J)}_{j_1 j_2}(c_k)$ is expected to be isotropic.

The matrix element $\langle V_3 \rangle$ can be well approximated by

$$\langle V_3 \rangle^2 = D_3[(E_T - E_{j_1} - E_{j_2})^2 + (\Gamma^J)^2/4]\,,$$

where the parameter $D_3 \approx 1.0 - 1.5$ (see Ref. [11] for details) and Γ^J, the three-body decay width, is obtained selfconsistently from the FWHM of the distribution specified by Eq. (2).

The differential flux dj in Eq. (2) is normalized so that the three-body decay width is obtained as

$$\Gamma^{(J)}_{j_1 j_2}(E_T) = \int_0^1 d\varepsilon \int_{-1}^1 dc_k \, \frac{dj^{(J)}_{j_1 j_2}(E_T)}{d\varepsilon \, dc_k}\,.$$

Typically for ground states there is only one configuration contributing significantly to the width, however for the 2^+ state, several configurations have non-negligible contributions and the total width is given by

$$\Gamma^{(J)}(E_T) = \sum_{j_1 j_2} W^{(J)}_{j_1 j_2} \Gamma^{(J)}_{j_1 j_2}(E_T)\,, \qquad (3)$$

where $W_{j_1 j_2}$ are the weights of different configurations in the wavefunction (WF).

B. Three-body calculations

The three-body ^{14}O+p+p cluster model for the ^{16}Ne decay was originally developed in Ref. [12]. Since that time our theoretical approach has developed considerably [1] including a careful consideration of the Thomas-Ehrmann effect [13] and a precise treatment of the decay dynamics and long-range Coulomb effects [2]. Reference [13] provides a detailed up-to-date description of the model used for these ^{16}Ne calculations.

III. ^{14}O+p+p EXCITATION SPECTRUM

Details of the experimental method has been described previously in Ref. [2]. Briefly, a secondary beam of $E/A = 57.6$ MeV (at the center of the target) ^{17}Ne, provided by the National Superconducting Cyclotron Laboratory, bombarded a 1-mm-thick ^{9}Be target. Following neutron knockout reactions, the ^{16}Ne decay products

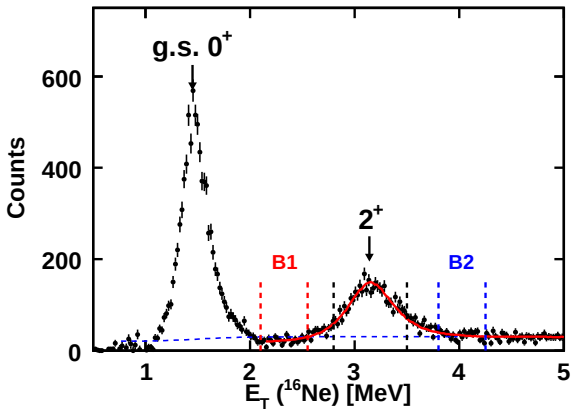

FIG. 2. (Color online) Distribution of ^{16}Ne decay energy determined from detected ^{14}O+p+p events showing peaks associated with the ground and first excited states of ^{16}Ne. The solid curve shows a fit to the first excited state where the dashed curves indicates the fitted background under this peak. Two background gates, $B1$ and $B2$, are shown which are used to investigate the background contributions to the measured decay correlations.

were detected in the HiRA array [14] consisting of 14 $\Delta E - E$ telescopes arranged around the beam to cover zenith angles from 2° to 13.9°. The double-sided Si strip ΔE detectors permitted accurate determination of the scattering angle of the detected fragments. Energy calibrations were achieved using beams of 55 and 75 MeV protons, E/A=73 and 93 MeV ^{14}O, and E/A=45.8 and 53.1 MeV ^{13}N projectiles. The relative locations of each HiRA telescope and the target were determined very accurately using a Coordinate Measurement Machine arm.

The distribution of ^{16}Ne decay energy E_T deduced from detected ^{14}O+p+p events via the invariant-mass method is displayed in Fig. 2. This spectrum has been corrected for a contamination from ^{15}O+p+p events where a small fraction of ^{15}O fragments have leaked into the ^{14}O gate in the $E - \Delta E$ spectrum. This correction is described in more detail in Ref. [2] where the raw uncorrected spectrum is also shown.

The ^{16}Ne ground-state peak at $E_T = 1.466(20)$ MeV dominates the spectrum, but in this work we will concentrate on the smaller peak at $E_T = 3.16(2)$ MeV which has an excitation energy of $E^* = 1.69(2)$ MeV. In the ^{16}C mirror nucleus, the lowest excited states are a 2^+_1 state at $E^* = 1.766$ MeV and a 0^+_2 state at $E^* = 3.027$ MeV [15]. If the excited state observed in this work is the 0^+_2 state, then this would correspond to a very large Thomas-Ehrman shift of 1.3 MeV that would be ~ 1 MeV larger than that for the ground state. Recent theoretical calculations of the Thomas-Ehrman effect for ^{16}Ne-^{16}C mirror partners [13] favor the 2^+ assignment providing consistent predictions for 0^+_1 and 2^+ state energies of ^{16}Ne simultaneously. The Thomas-Ehrman shifts predicted in [13] for ^{16}Ne 0^+_1 and 2^+ states are around $200 - 300$ keV.

Therefore we believe this state is the mirror of the 2^+_1 first excited state of ^{16}C. The energy of this peak is close to other levels observed in previous experiments, see the discussion of Sec. VII.

IV. WIDTH OF THE 2^+ STATE

Figure 2 shows a fit to the 2^+ peak using a Breit-Wigner line shape where the effects of the experimental resolution (and its uncertainty) are included via Monte Carlo simulations as described in Ref. [2]. The fit is shown by the solid line while the dashed curve indicates the fitted smooth, almost flat background. This fit is not unique as different functional forms of the background could be assumed. However, the relative magnitude of the background is small and the dependence on the exact form of the background is not large (see below). The extracted intrinsic width in this particular fit is $\Gamma = 150(50)$ keV where the error bar results predominately from the uncertainty associated with the effects of energy loss and small-angle scattering of the decay products in the target. See Ref. [2] for a discussion for this uncertainty. Upper limits to the width of this state were also obtained from the other neutron knockout experiments. Our extracted width is consistent with $\Gamma = 200(200)$ keV obtained in Ref. [6], but inconsistent with the limit of $\Gamma \leq 50$ keV from Ref. [7], see further discussion in the Section VII.

We have explored whether other choices of the background shape could result in significantly smaller values of Γ. If the background has a minimum under the peak, the extracted width would be smaller if the intrinsic width of this minimum was less than 200 keV. Such a narrow "V"-shaped background seems unlikely, but in any case the depth of the such a minimum is limited as the intrinsic background (before the effects of detector resolution is applied) must always be positive. With this constraint, the observed background, after the effects of the experimental resolution is included, is always quite shallow for such narrow "V" backgrounds and produces a negligible change in the extracted value of Γ. On the other hand the use of wide "V"-shaped background can increase the extracted width. We estimate the maximum value of Γ from this and other uncertainties is 250 keV and finally we obtain $\Gamma = 175(75)$ keV.

A. Three-body calculations

For the ground state of ^{16}Ne, our three-body calculations predict $\Gamma = 3.1$ keV which was found to be consistent with the upper limit we extracted for the intrinsic width of $\Gamma < 80$ keV [2]. Moreover, the model reproduces the experimental momentum correlations between the decay products with high precision. The decay mechanism of this state is the so-called true three-body decay

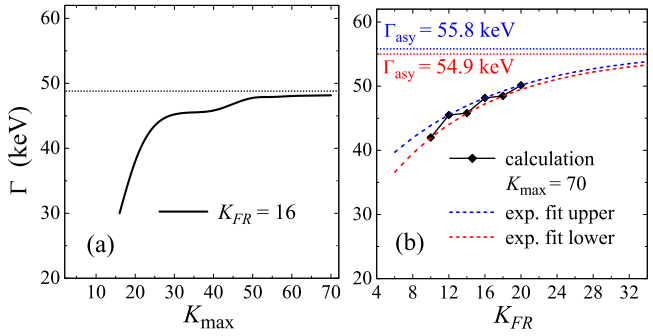

FIG. 3. (Color online) Convergence of the width calculations for the ^{16}Ne 2^+ state. (a) $K_{\max}$ convergence at a fixed K_{FR}. (b) K_{FR} convergence at a fixed $K_{\max}$. Exponential extrapolations (separately done for odd and even $K_{FR}/2$ values) point to a width of around $\Gamma = 56$ keV.

and as expected the hyperspherical method delivers very accurate results in this case.

The 2^+ state of ^{16}Ne can decay sequentially via the ^{15}F $s_{1/2}$ g.s. at $E_r \approx 1.4$ MeV and the first-excited, $d_{5/2}$ state at $E_r = 2.80$ MeV (see Fig. 1). The hyperspherical method is not as well suited for width calculations of states with important sequential decay channels and thus special care is required for the 2^+ calculation. For this level, the three-body calculations predict an intrinsic width of $\Gamma = 51$ keV for the largest basis size considered. The basis convergence of this result is studied in Fig. 3. The basis size is defined by $K_{\max}$, the maximum value of the principle quantum number K in the hyperspherical method. In our calculations, large basis sizes become available with the help of an adiabatic procedure ("Feschbach reduction", see e.g. Ref. [10]) that converts the calculation to one with a smaller basis size K_{FR}, which is then treated in a fully dynamical manner. It can be seen from Fig. 3(a), that $K_{\max}$ convergence for a given K_{FR} is quite convincing. In contrast, K_{FR} convergence is not complete and displays some odd-even staggering with respect to $K_{FR}/2$. To estimate the final converged width at large K_{FR}, we performed exponential extrapolations separately for both odd and even $K_{FR}/2$ values [Fig. 3(b)]. The extrapolations provided very similar asymptotic values of $\Gamma \sim 56$ keV. Thus we regard this as the correct theoretical prediction. This value is smaller than the experimental result $\Gamma = 175(75)$ keV, and we do not see how the three-body calculations could be improved to match the experimental value.

B. Simplified decay model estimates

To investigate whether larger theoretical widths are possible, we performed calculations using the simplified decay model of Eq. (2). For the estimates provided in Table I, we have chosen parameter sets in a reasonable way, by stretching all of them in the direction maximiz-

ing the width estimate. The channel radius $r_{\rm ch} = 4.25$ fm and the reduced width $\theta^2 = 1.5$ were used for all core+p resonances. The energies of the $p_{1/2}$ and $p_{3/2}$ resonances were assigned assuming isobaric symmetry between ^{15}F and ^{15}C states. The assumed energy of the $d_{3/2}$ resonance $E_{d_{3/2}} = 8$ MeV is also the minimal value which does not contradict the spectrum of ^{15}C.

The structure information on the $J^\pi = 2^+$ ^{16}Ne state in Table I is taken from Ref. [13]. However, for this table we required a more detailed decomposition than was provided in the original work. In spite of the simplicity of the model, the total width of the 2^+ state evaluated according to Eq. (3) is found to be around $\Gamma = 51$ keV in a good agreement with the three-body calculations of Sec. IV A.

As shown in Table I, there are two ways to increase the estimated width: (i) decrease in the energy E_r of the ^{15}F $s_{1/2}$ ground state or (ii) drastically increase the $[s_{1/2}d_{5/2}]_{2^+}$ configuration weight. In both cases, the calculated widths remain at the lower limit of the experimental uncertainty. In evaluating these possible modifications one should consider their consistency with structure of the mirror states. The Thomas-Ehrman effect and the Coulomb displacement energies for the 0^+ and 2^+ states of the ^{16}Ne-^{16}C isobaric mirror partners were studied in detail in Ref. [13]. A sensitive relationship was found between the energies of the 0^+ and 2^+ states, their structures, and the ^{15}F $s_{1/2}$ ground-state energy. The latter was fixed in the calculations [13] at $E_r = 1.405(20)$ MeV using our experimental values for the ground and 2^+ states of ^{16}Ne [2]. It is very difficult to drastically change the spin structure of predicted WF without a catastrophic effect on the consistency with the experimental energies of the 0^+ and 2^+ states achieved in Ref. [13]. Thus, a complete revision of our theoretical understanding of ^{16}Ne and ^{15}F systems is required to allow realization of variants proposed in (i) and (ii).

C. Outlook for 2^+ state width

Given that the experimental width of the 2^+ state is larger than expected, it is useful to examine if there could be additional contributions to the ^{16}Ne excitation spectrum which overlap with the 2^+ state. One such possibility is that the peak we observed is actually a doublet with contributions from both the 2^+_1 and the 0^+_2 levels. Föhl *et al.* [8] report a 0^+_2 excited state at $E^* = 2.1(2)$ MeV [with corresponding $E_T = 3.57(20)$ MeV] in the ^{16}O(π^+,π^-) reaction. This energy is a 2σ difference from our fitted centroid, but overlaps with the observed peak.

In our three-body calculations [2], the 0^+_2 state is predicted in the range $E_T = 4.3 - 4.6$ MeV, well separated from the observed peak and consistent with the energy of the $E^* = 3.03$-MeV state in ^{16}C which is expected to be the 0^+_2 mirror partner. Furthermore, the three-body calculations of Ref. [2] indicate that the 0^+ excitation function for ^{16}Ne has a dip, and not a peak, at the predicted energy of the 0^+_2 state. In these ^{17}Ne$(-n) \rightarrow ^{16}$Ne neutron-knockout calculations , the 0^+_2 state is strongly suppressed as the overlap of the valence-proton configurations for the ^{17}Ne ground state with those of the ^{16}Ne ground state (0^+_1 state) is so strong that there is little room for yield from the 0^+_2 state. We regard this assumed ^{17}Ne structure as quite realistic as it was found to lead to an excellent agreement with a broad range of observables [16]. Of course, the ^{17}Ne structure or the reaction mechanism maybe more complicated than assumed in our calculations and the data of Föhl *et al.* and the calculations of Ogawa *et al.* [17] suggest that the location of this state could be much closer to our observed peak. In summary, it is clear that we do not fully understand the magnitude of the width of the 2^+ state and that this issue is strongly related to excitation energy of the 0^+_2 state and its population in these neutron knockout reactions.

V. CORRELATIONS FOR 2^+ STATE

The experimental two-dimensional Jacobi "Y" and "T" correlations for the 2^+ state are shown in Figs. 4(a) and 4(d), respectively. The E_T gate used to select this peak is indicated in Fig. 2. Both distributions show the presence of two ridge structures, and indeed double-ridge structures are expected for sequential decay. The location of these ridge structures along the Jacobi "Y" energy axis correspond qualitatively to those expected from the decay via the $s_{1/2}$ ground state of ^{15}F with $E_r \sim 1.4$ MeV. However, these ridge structures are very pronounced and intense only in the diproton halves of the distributions [small ε in the Jacobi "T" or negative $\cos(\theta_k)$ in the Jacobi "Y" distribution]. For the other halves of the distributions, the overall intensity is reduced

TABLE I. Simplified-decay-model estimates of important configurations of the ^{16}Ne 2^+ WF for D_3=1.0. The total decay width according to Eq. (3) is provided in the line "Total". The sensitivity of the three-body width to variations of the ^{15}F g.s. energy is illustrated by the three bottom lines of the Table.

$[l_{j_1}l_{j_2}]_{J^\pi}$	$W^{(2)}_{j_1j_2}$ (%)	E_{j_1} (MeV)	E_{j_2} (MeV)	$\Gamma^{(2)}_{j_1j_2}$ (keV)
$[p_{1/2}p_{3/2}]_{2^+}$	3.0	4.5	6.0	11
$[p^2_{3/2}]_{2^+}$	1.1	6.0	6.0	7
$[d^2_{3/2}]_{2^+}$	1.2	8.0	8.0	0.04
$[d^2_{5/2}]_{2^+}$	5.4	2.8	2.8	1.6
$[s_{1/2}d_{3/2}]_{2^+}$	71.3	1.4	8.0	50
$[s_{1/2}d_{5/2}]_{2^+}$	15.9	1.4	2.8	93
Total	97.9			50.9
$[s_{1/2}d_{5/2}]_{2^+}$	15.9	1.2	2.8	113
$[s_{1/2}d_{5/2}]_{2^+}$	15.9	1.3	2.8	103
$[s_{1/2}d_{5/2}]_{2^+}$	15.9	1.5	2.8	89

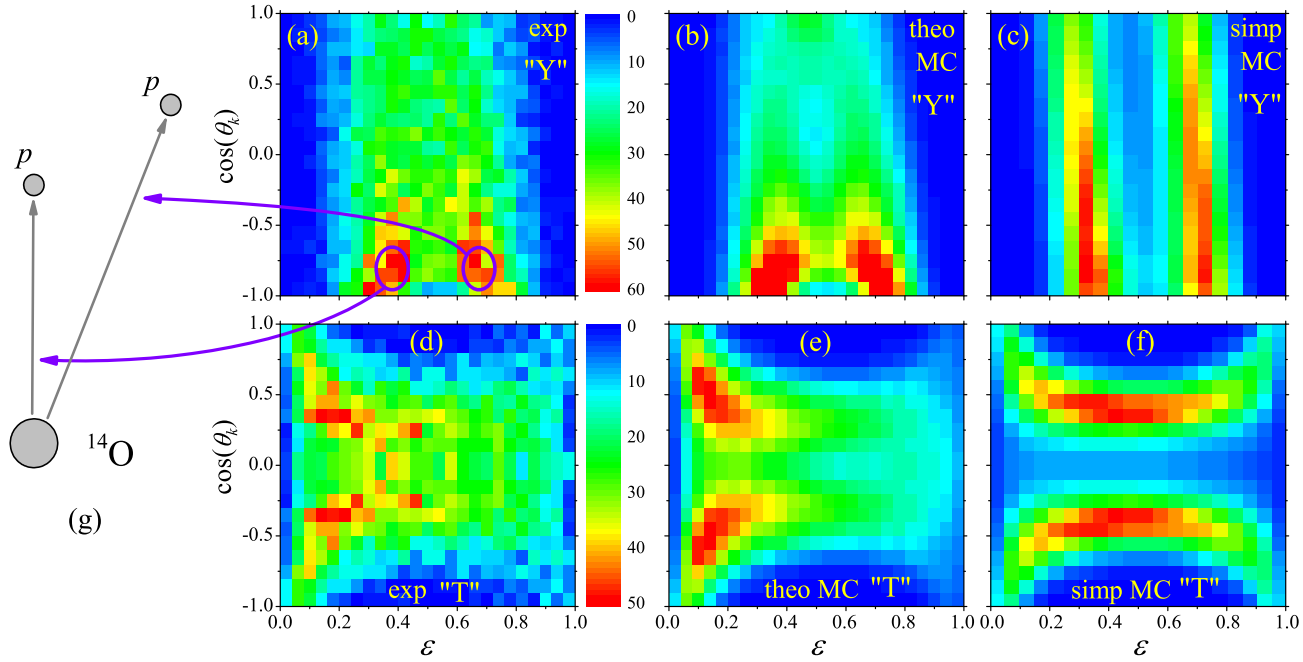

FIG. 4. (Color online) Comparison of the experimental Jacobi (a) "Y" and (d) "T" correlation distributions to the those of the three-body model [(b) and (e)] and those from a sequential decay simulation [(c) and (f)]. The effects of the detector efficiency and resolution in the theoretical distributions have been included via Monte Carlo simulations. (g) Shows the relative orientation and magnitude of the two proton velocity vectors for the peak regions indicated by blue circles in panel (a).

and the ridge structures have largely faded out. These features can also be seen in the projected energy distributions for the two Jacobi systems plotted in Figs. 5(a), 5(c), and 6. The geometry of the most probable decay configurations, associated with the more intense regions of the ridges, is illustrated in Fig. 4(g) (left).

A. Background contribution to correlations

Before discussing the correlations from our two models, it is useful to consider the contributions of the background under the $J^\pi = 2^+$ peak. From the fit shown in Fig. 2, we estimate that our energy gate spanning the excited-state peak contains a 24% background contribution. Background gates, $B1$ and $B2$, were placed either side of this peak (see Fig. 2) to investigate the correlations associated with this background. The number of events in these background gates is too small to obtain useful information from the two-dimensional distributions, so we will concentrate on the projected distributions. The projected energy distributions in both the "T" and "Y" systems are compared for the main and background gates in Figs. 5(a) and 5(c). The results for the each background gates have been normalized to 24% of the peak yield and the error bars are too small to be seen as they are less than the size of the data points.

We should emphasize here that the "background" is expected to be largely a "physical background" from decay of unresolved ^{16}Ne states. For example, based on the theoretical calculations of Ref. [2], the $B1$ gate contains contributions from the large high-energy tail of the ground state and the $B2$ has contributions from a wide 1^- state.

For the Jacobi "Y" system shown in Fig. 5(a), there are significant differences between the two background distributions. The $B2$ distribution has a double-peak structure much like that obtained for the excited-state gate, but the two peaks are separated further apart in energy as would be expected for sequential decay of a higher-lying ^{16}Ne level decaying through the ^{15}F ground state. In fact, the peak locations roughly match the expectation from a sequential calculation with the simplified model (Sec. V B) which are indicated by the arrows. For the $B1$ gate, there is only a single peak at $\varepsilon \sim 0.5$, but this is expected from Eq. (2) for a such small E_T value. If the energy projection for the background under the peak is intermediate between the $B1$ and $B2$ projections, then it will have a two-peak shape similar to the peak-gated projection. Note the magnitude of the two peak structure in the peak-gated distribution is too large to be entirely due to this background, therefore the presence of the background only contributes moderately to this feature.

On the other hand for the Jacobi "T" system in Fig. 5(c), the two background distributions are quite similar and therefore it is reasonable to assume the background under the peak has a similar, almost flat, dependence.

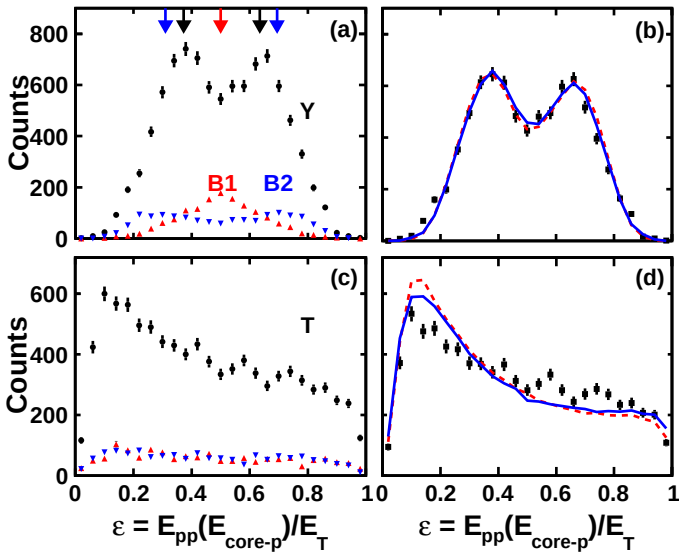

FIG. 5. (Color online) Comparison of projected Jacobi (a) "Y" and (c) "T" energy distributions for peak-gated events and the events in the neighboring background gates $B1$ and $B2$. In (b) and (d) the experimental projections have been background subtracted (see text) and are compared to the predictions of the three-body model before (dashed curves) and after (solid curves) the effects of the detector bias and acceptance was included. The arrows in (a) show the predicted locations of the maxima from Eq.(2) for the mean energies of each of the three gates.

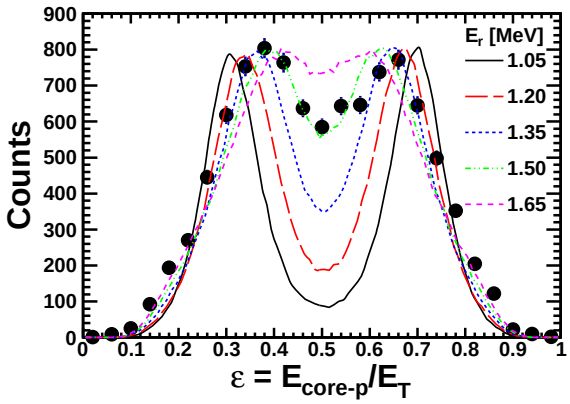

FIG. 6. (Color online) Experimental energy distribution for ^{16}Ne 2^+ state in the "Y" Jacobi system (data points) is compared with distributions calculated by the R-matrix-type expression of Eq. (2) for the different $s_{1/2}$ g.s. resonance energies E_r in ^{15}F listed in the figure. The detector efficiency and resolution were included via the Monte Carlo simulations.

As such, its contribution does not alter the measured distribution significantly. The data in Fig. 5(d) shows the Jacobi "Y" energy distribution after the average of the $B1$ and $B2$ gates are subtracted. It is not significantly different from the original distribution in Fig. 5(c). A similar subtraction is also made for the Jacobi "Y" distribution in Fig. 5(b), but in this case it is not clear how appropriate this is. However, the change in shape from the original distribution in Fig. 5(a) is again minor.

If the observed $E_T = 3.15$ MeV peak is a doublet, as discussed in Sec. IV C, and the correlations for the two states are different, then one might see an E_T dependence of the correlations within the E_T range of the peak. No evidence for such an effect was observed. The only observed dependence of statistical significance is small shifting of the energies of the two peaks which follows the expected E_T dependence for decay through the ^{15}F ground state.

B. Correlations in the simplified model

In the simplified model [Eq. (2)], the double-ridge distribution of Fig. 4(a) is dependent on the energy E_r of the ground state $s_{1/2}$ resonance in ^{15}F. However, this energy is not very well defined experimentally with results varying from 1.23 to 1.52 MeV, see e.g. the discussion and references in Refs. [13, 18]. Figure 6 demonstrates the strong sensitivity of the simplified model to the value of E_r. This result, for the first excited state, is in stark contrast to the ground state where we found the "Y" system energy distribution was insensitive to realistic variations of E_r. The range of E_r consistent with the data in Fig. 6 is $1.4 \lesssim E_r \lesssim 1.5$ MeV which is also consistent with the range $1.39 \lesssim E_r \lesssim 1.42$ MeV determined from an analysis of Coulomb displacement energies [13]. Also see the discussion of the ^{15}F ground state in Sec. IV B.

A detailed view on the correlations from the simplified model is presented in the two-dimensional distributions shown in Figs. 4(c) and 4(f). These distributions were calculated with $E_r = 1.405$ MeV [13] and the effects of the detector efficiency and resolution were included via the Monte Carlo simulations. Both distributions show the expected double-ridge structures. The sequential aspect of the decay is most easily understood in the Jacobi "Y" distribution of Figure 4(c). Here the two-ridge structures are prominent over the whole angular range. The angular distribution functions $f^{(J)}_{j_1 j_2}(c_k)$ are isotropic for all the contributions in Table I except for the minor $[p^2_{3/2}]_{2^+}$ and $[d^2_{5/2}]_{2^+}$ components. Therefore ridges are predicted to have uniform intensity as a function of $\cos(\theta_k)$ and the small dependence seen in Fig. 4(c) is just due to the detector acceptance. The use of smaller values of E_r in these simulations would result in the same basic picture, but the separation between the ridges would be increased and the match with the experimental ridges at low ε values would be worse.

Comparing the data and sequential simulations, we find that the experimental distribution looks sequential only in the regions were there are strong p-p final-state interactions suggesting that the decay is sequential only

when it is also of diproton nature and vice versa which seems nonsensical. The "diproton" regions are those with small ε in "T" system and $\cos(\theta_k) \sim -1$ for medium ε values in "Y" system. The actual geometry of the most probable decay configuration is visualized in Figure 4(g). Clearly the decay mechanism is more complicated than this intuitively-simple sequential picture.

The apparent conflict between features that look sequential in the "Y" energy distribution and features indicating strong p-p final-state interactions in the "T" energy distribution was also noted in the decay of highly-excited states of ^{6}Be [4]. As the ^{6}Be results are qualitatively consistent with the present work, then it seems that the detailed structure of the state and the magnitude of the Coulomb barriers are not responsible for explaining these unusual correlations.

C. Comparison with three-body calculations

The predicted two-dimensional correlations from the three-body model, after the effects of detector bias and resolution are included via the Monte Carlo simulations, are shown in Figs. 4(b) and 4(e) for the two Jacobi systems. These three-body calculations reproduce the major features of the experimental results. Like the experimental data, the "sequential-decay" ridges are clearly present and pronounced only in the diproton region. The agreement is not perfect. For example, the three-body calculations predict a "hole" in two-dimensional distributions that is most obvious in the Jacobi "Y" distribution of Fig. 4(b) where it is centered at $\{\varepsilon = 0.5, \cos(\theta_k) \sim 0.3\}$. This feature, if present at all in the experiment data, is significantly reduced. However, it should be noted that the experimental distribution are expected to contain $\sim 24\%$ background which will make such a fine feature difficult to see.

More detailed quantitative comparisons are made in Figs. 5(b) and 5(d), where the projected energy distributions are compared to the data. The predictions before and after accounting for the effects of the detector bias and resolution are similar as indicated by the dashed and solid curves, respectively. The two-peak structure is well reproduced in the projection for the Jacobi "Y" distribution in Fig. 5(b). In the Jacobi "T" distribution of Fig. 5(d), the three-body model also predicts an appropriate enhancement of the diproton region (small ε), but the magnitude of the effect is somewhat larger than that observed experimentally. A similar result was obtained for the the highly-excited continuum of ^{6}Be [4]. We note that computation of the "Y" ε distribution is more sensitive to model parameters like the resonance energy E_r of ^{15}F ground state. In contrast, the "T" ε distribution is much less sensitive to these parameters and very stable in various computation conditions. It is also possible that this disagreement maybe related to uncertainties in the background contribution, but the "T" background seems better constrained than the "Y" background (Sec. V A).

VI. DECAY MECHANISM FOR 2^+ STATE IN THREE-BODY CALCULATIONS

The three-body calculations reproduce the diproton and sequential features of the experimental distributions. In order to better understand the origin of these unusual momentum correlations we have examined the radial evolution of the decay WF $\Psi^{(+)}$. Figure 7 shows the correlation density

$$W(\rho, \theta_\rho) = \int d\Omega_x \, d\Omega_y \, |\Psi^{(+)}(\rho, \theta_\rho, \Omega_x, \Omega_y)|^2$$

as a function of the hyperangle and hyperradius in the Jacobi "Y" system. The Jacobi vectors $\mathbf{X}$ and $\mathbf{Y}$ in this system, illustrated in Fig. 7(c), are defined via the hyperspherical variables as

$$\rho^2 = \tfrac{A_1 A_2}{A_1+A_2} X^2 + \tfrac{(A_1+A_2)A_3}{A_1+A_2+A_3} Y^2 = \tfrac{14}{15} X^2 + \tfrac{15}{16} Y^2 \,,$$

$$X = \rho \sqrt{\tfrac{A_1+A_2}{A_1 A_2}} \sin(\theta_\rho) = \rho \sqrt{\tfrac{15}{14}} \sin(\theta_\rho) \,, \qquad (4)$$

$$Y = \rho \sqrt{\tfrac{A_1+A_2+A_3}{(A_1+A_2)A_3}} \cos(\theta_\rho) = \rho \sqrt{\tfrac{16}{15}} \cos(\theta_\rho) \,, \qquad (5)$$

where in the "Y" system $A_1 = A_{core}$ and $A_2 = A_3 = 1$. The mid point of the θ_ρ-axis in Figs. 7(a,b) approximately corresponds to symmetric configurations of the valence nucleons, i.e.

$$\theta_\rho \sim \pi/4 \quad \rightarrow \quad X \sim Y \sim \rho/\sqrt{2} \,.$$

For large ρ values, the coordinate-space hyperangle θ_ρ transforms into momentum-space hyperangle $\theta_{\varkappa}$ defining the energy distribution between the subsystems:

$$\theta_\rho \rightarrow \theta_{\varkappa}, \quad E_x = E_T \sin^2(\theta_{\varkappa}), \quad E_y = E_T \cos^2(\theta_{\varkappa}). \qquad (6)$$

Thus the representation of Figs. 7(a,b) best illustrates the geometry of the single-particle configurations.

The population density in Fig. 7(a) is very large for typical nuclear dimensions $\rho < 5$ fm where the two protons are inside the Coulomb barrier. This indicates the region of resonant-state formation. Extending out from this region are ridges associated with different decay paths.

Classical trajectories for sequential decay, differing in the decay time of the ^{15}F intermediate state are indicated by the dashed (blue) arrows. The initial portion of these trajectories is common to all sequential decays (one of the protons is emitted while the other remains close to the core) and they follow lines of roughly constant, but small, values of either X or Y. The presence of the ridges in Fig. 7(a), which are roughly parallel to the yellow lines shown for constant $X = 2.5$ or $Y = 2.5$ fm, confirms that there is a sequential component in these three-body calculations. The classical trajectories deviate from these ridges when the second proton is emitted and at this stage the classical trajectories diverge and so this part of the decay is not reflected by a ridge structure in the WF and thus is less visible. However, the decay paths do

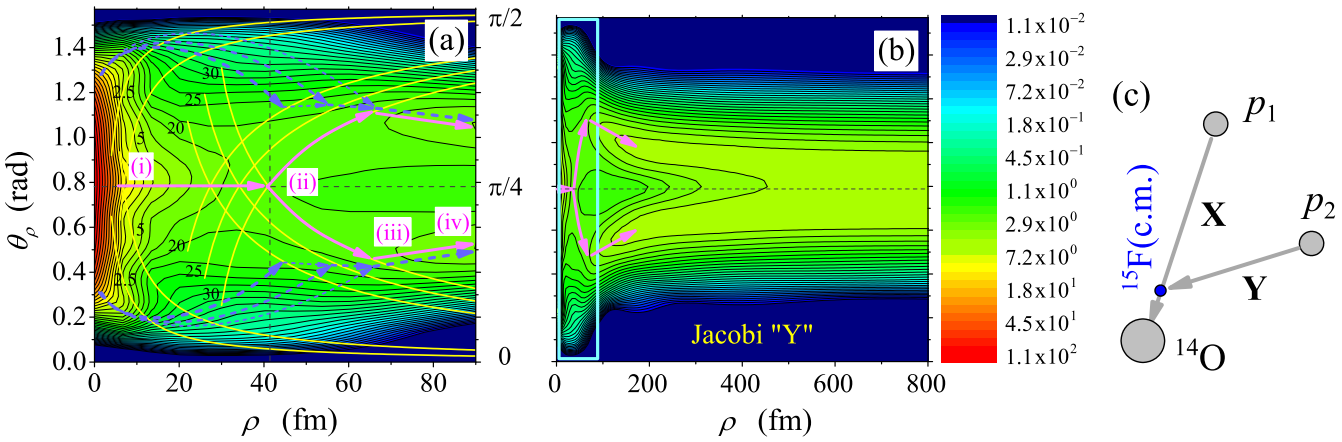

FIG. 7. (Color online) Correlation density $W(\rho, \theta_\rho)$ for ^{16}Ne 2^+ state WF $\Psi^{(+)}$ in the "Y" Jacobi system. Panels (a) and (b) show the evolution of the predicted hyperangular distribution with hyperradius on two different scales. Yellow curves in (a) provide the levels with constant absolute values of **X** and **Y** vectors indicated by the attached numbers (in fm). Blue (dashed) and pink (solid) arrows qualitatively indicate the classical paths connected with sequential and the "tethered" decay mechanisms correspondingly. The blue frame in the panel (b) shows the scale of panel (a). Panel (c) illustrates the arrangement of the **X** and **Y** vectors for the "Y" Jacobi system, see Eqs. (4) and (5).

eventually concentrate at larger ρ values along the two well-defined ridges which are clearly seen in Fig. 7(b).

The other prominent penetration path in the three-body calculations, schematically indicated by solid (pink) arrows, is more unusual. One observes a well-defined ridge in the range (i)-(ii) in Fig. 7(a) extending out from the main concentration of contours. For this ridge, $X \sim Y$ and thus the protons are penetrating the barrier simultaneously. The density in this ridge within the range (i)-(ii) again decreases exponentially with ρ. Simultaneous emission of protons is of course a well established decay mechanism [1]. However, the emission dynamics changes in the range (ii)-(iii). Here the arrows more closely follow the lines of constant X and Y which means that radial motion of one of the protons is now practically stopped (much slower than the orbital motion), while the other continues to move in the radial direction. Finally in the range (iii)-(iv) are two symmetric ridges which smoothly evolve with ρ to the "sequential-decay" double-hump structures observed in the energy distribution of Fig. 5(b). This region is common for both the initial sequential and prompt decay paths and both protons are more or less in the state of free flight except for the effect of the long-range Coulomb interaction. This behavior implies that in the evolution along the path (i)-(iv), the "near" proton leaves its position adjacent to the core at point (iii) starting the expansion stage of the whole system. At this moment even the "near" proton is already far beyond the typical nuclear size relative to the core and thus the WF component evolving along the (i)-(iv) pathway cannot "remember" information about core-p interaction. However, the sequential trajectories merge with this decay path at this point and from Eq. (6), the "near" proton and core have the relative energy appropriate for the ^{15}F ground-state resonance. Thus we conclude that the expansion stage (iii)-(iv) is initiated for this WF component by the interference with WF components associated with the sequential decay path [dashed (blue) arrows] which "contain" such an information.

The information on angular distributions of **X** and **Y** vectors is integrated for presentation of Fig. 7. The analysis of the WF for the "pink trajectory" region indicates that this angular distribution is quite broad with a mean angle between **X** and **Y** close to $\pi/2$. The average case of the solid (pink) path from Fig. 7 is visualized in Fig. 8. In the three-body decay plane ($r_z = 0$), the initial trajectories of protons are directed along r_x and r_y axes. The line $r_x = r_y$ corresponds to the trajectory of the center of mass of the p-p subsystem. It can be seen that at distances of about 30 fm, the radial propagation of one of the protons is practically stopped and the protons behave for some time as connected with a kind of "tether" of (practically) fixed length (blue dotted lines in Fig. 8) producing complicated spatial trajectories. The realistic motion in our quantum-mechanical calculations does not of course correspond to this piecewise trajectory; quantum mechanical motion is always "smooth" and there are no well defined decay paths as in the classical case. However, this idealized decay path is quite instructive and demonstrates the complexity of this decay that we portray in qualitative terms as a "tethered decay mechanism".

VII. PREVIOUS EXPERIMENTAL STUDIES

In 1978 KeKelis *et al.* [19] reported the detection of the first excited state of ^{16}Ne from the observation of a

peak with yield of ~ 12 counts at $E_T = 3.03(7)$ MeV in the ^{20}Ne(^{4}He,^{8}He) reaction.

More recently, information on the lowest ^{16}Ne excitations was obtained in two studies [6, 7] which also used neutron knockout from ^{17}Ne beams, but at relativistic energies. See Table II for a comparison of extracted centroids and widths for the ground and first-excited states in these and the present of experiment.

The work of [6] uses a technique based on the tracking of the reaction products that was created for studies of the radioactive decay lifetimes in the fs-ns range. In the case of the much shorter-lived ^{16}Ne states, the lifetime information is not extractable. The spectroscopic properties are obtained in this model based on kinematically incomplete information. Therefore the resonance parameters are recovered by MC simulations based on theoretical assumptions about spectrum populations and decay mechanisms and have large uncertainties. The ^{16}Ne g.s. position $E_T(0^+) = 1.35(8)$ MeV found in [6] has a value which is somewhat lower than ours, but otherwise the results are consistent.

The ^{16}Ne excitation spectrum measured in Refs. [7, 20] is very similar to ours. This is evidence for a similar reaction mechanism despite the large differences in bombarding energies: $E/A = 500$ MeV compared our value of $E/A = 57.6$ MeV. The experimental resolution and statistical uncertainty in Refs. [7, 20] are significantly worse than in our present work [2], the former can be gauged by the widths of the experimental peaks which are almost a factor of two larger than those in Figure 2. Despite these difference, it is surprising that the uncertainties on the extracted widths from Refs. [7, 20] are smaller than ours. Such an extraction would require an extremely precise understanding of their experimental resolution. The 2^+ decay energy E_T in Refs. [7, 20] is consistent within the listed experimental errors to our value, but the extracted width in these references ($\Gamma < 50$ keV) is inconsistent with the present work.

Correlation data for the 2^+ state in this relativistic study were also presented in Ref. [20] and it was concluded that they are consistent with a purely sequential calculation. No two-dimensional correlation plots are shown in Ref. [20], however, projections on the energy and angular axes are presented (see Fig. 8 of [20]). Their energy distribution in the "Y" system does not have the doubled-humped structure present in the distribution of Fig. 5(a). However, if we take our best-fit simplified-model calculation or the three-body model result and artificially decrease the experimental resolution in our MC simulations so as to reproduce the experimental width of the 2^+ state in the relativistic study, then this feature is washed out and one is left with a broad peak similar to that found in Ref. [20].

The energy distribution in the "T" system obtained from the study of Ref. [20] is consistent with their flat sequential calculation within the large statistical error bars. However, it is also clear that a dependence with enhanced correlations in the diproton region of similar magnitude to that found in our distribution in Fig. 5(b) would also be consistent. Therefore, the two sets of experimental data may not be inconsistent, however more precise comparisons would require a detailed knowledge of the experimental acceptance of Ref. [20]. It seems that the higher resolution and statistics of the present work have permitted us to better characterize the decay mechanism and allow the non-sequential aspects of the decay to become clearer.

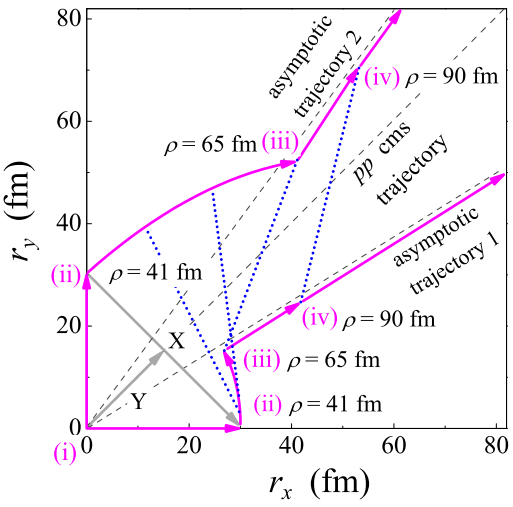

FIG. 8. (Color online) Schematic of the tethered decay mechanism. Trajectory of two protons corresponding to solid (pink) path in Fig. 7. The configurations labeled by the Roman numerals correspond to the same configurations denoted in Fig. 7. The p-p center-of-mass motion path $r_x = r_y$ is collinear with $\mathbf{Y}$ vector for the Jacobi "T" coordinate system.

VIII. HIGHER EXCITED STATES

In Ref. [2] we also reported on the a second excited state in the ^{14}O+p+p channel at $E_T = 7.60(4)$ MeV. This peak was relatively weak in our excitation spectrum (due to its lower detection efficiency) so no further analysis

TABLE II. The properties of 0^+ g.s. and first 2^+ states of ^{16}Ne obtained in the recent neutron knockout reaction studies with ^{17}Ne beam. Energies and widths are in MeV. All the E_T values are provided relative to the ^{14}O+p+p threshold.

Work	[6]		[7]		[2], this work	
J^π	E_T	Γ	E_T	Γ	E_T	Γ
0^+	1.35(8)		1.388(15)	0.082(15)	1.466(20)	< 0.08
2^+	3.2(2)	0.2(2)	3.220(46)	< 0.05	3.160(20)	0.150(50)
(2^+)	7.6(2)	$0.8^{+0.8}_{-0.4}$	7.57(6)	≤ 0.1	7.60(4)	≤ 0.5
(?)					9.84(10)	0.32(10)
(?)					12.23(20)	0.51(23)

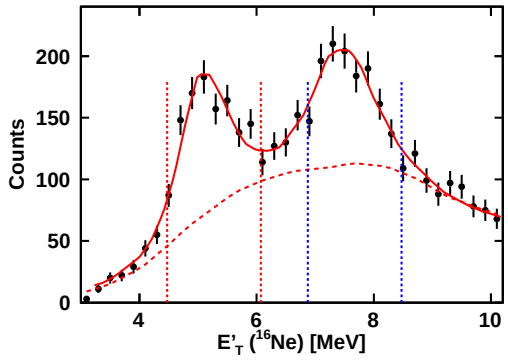

FIG. 9. (Color online) Distribution of ^{16}Ne decay energy determined from detected ^{13}N+p+p+p events. Gates are shown on the two observed peaks which are used in the analysis shown in Figure 10.

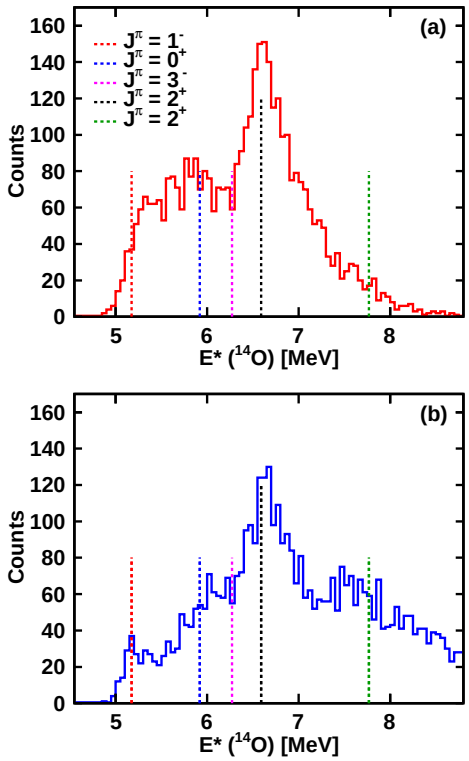

FIG. 10. (Color online) Distribution of ^{14}O decay energy determined for all possible ^{13}N+p subsets of each detected ^{13}N+p+p+p event. Pannel (a) is for the gate on the E'_T = 5.21 MeV state in ^{16}Ne while (b) is for the E'_T = 7.60 MeV state. The vertical dashed lines show the location of the first five excited states in ^{14}O.

was attempted. Even higher ^{16}Ne excited states were observed in Ref. [6] by their feeding into the states of ^{15}F. However, it was not possible to resolve them in this experiment.

At these higher excitation energies the decay will also start populating the ^{13}N+p+p+p exit channel (corresponding energy above its threshold is denoted as E'_T, see Fig. 1). The decay-energy spectrum for this channel is shown in Fig. 9 and displays two peaks at E'_T = 5.21(10) and 7.60(20) MeV corresponding to ^{16}Ne excitation energies of E^* = 8.37(10) and 10.76(20) MeV, respectively. The solid curve shows the best fit for one choice of the background contribution (dashed curve). As for the ^{14}O+p+p channel, the fit assumes intrinsic Breit-Wigner line shapes where the effect of the experimental resolution is incorporated via the Monte Carlo simulations. The background is relatively large and other functional forms can give good fits as well. We have included contributions to the uncertainties of the peak energies based on fits with other background choices. The fitted intrinsic widths of these peaks were found be Γ = 320(100) keV and 510(230), respectively.

With three protons in the exit channel, it is much more difficult to determine the decay mechanism compared to channels with just two protons, especially given the relative large background contribution. However some information on the decay path can be established. Figure 10 shows the ^{14}O excitation reconstructed from the core and one of the detected protons for each of the two peaks in Fig. 9 using the gates shown by the dashed vertical lines. The location of the first five excited states in ^{14}O are shown by the vertical dashed lines in this figure. In interpreting these spectra, one must remember that more than half of the events come from background below the peaks. Also as only one of the three detected protons can come from the decay of an excited ^{14}O intermediate state, then at least 2/3 of the remaining yield in these spectra is an additional background. Although we cannot rule out small contribution from each of these ^{14}O states in Fig. 10, a peak associated with the forth excited state at E^* = 6.59 ($J^\pi = 2^+$) is quite prominent for both ^{16}Ne gates. Of course it is not entirely clear whether this ^{14}O level is associated with the background or the peaks in the ^{16}Ne spectrum. However, we note that gating on this $J^\pi = 2^+$ ^{14}O peak, strongly enhances the E'_T = 5.21 MeV ^{16}Ne peak and thus we feel confident that this 2^+ level is an important intermediate state in the decay of this level. A similar search for possible ^{15}F intermediate states was fruitless probably because such states are expected to be wide at the available ^{15}F excitation energies in these decays.

IX. CONCLUSIONS

The decay of the first excited state of ^{16}Ne has been studied both experimentally and theoretically. A peak located at decay energy E_T = 3.16 MeV was observed in the ^{14}O+p+p invariant mass spectrum which is consistent with the expected location of the 2^+_1 first excited state based on the better known spectroscopy of the mirror nucleus ^{16}C. The intrinsic width of this state was determined to be between 100 and 250 keV.

Three-body calculations which reproduced the momentum correlations of the ^{14}O+p+p decay products of the ground state and were consistent with the experimental limits for its intrinsic width were found to predict an intrinsic width for the 2^+_1 state of $\Gamma \sim 56$ keV which is smaller than the experimental range. This conflict suggests either some deficiency in the calculations or the possibility that the observed peak has other contributions, for example, from the second 0^+_2, state.

We have provided a detailed view of the decay mechanism for the $2p$ decay of the ^{16}Ne 2^+ state. This differs drastically from the common ideas about the decay process in terms of sequential or/and diproton decay mechanisms. The two-dimensional correlations measured for the $2p$ decay of the first excited state shows a double-ridge pattern expected for sequential decay only when the two protons have low relative energy (diproton-like correlation). A careful investigation of the decay mechanism on the level of the wavefunction in our three-body model indicates that the real situation is quite intriguing. The model predicts both sequential and prompt-decay paths which interfere and produce the strange decay pattern which we qualitatively describe as a "tethered decay mechanism". The observed correlation pattern is qualitatively similar to that measured previously for excited ^{6}Be fragments and suggests other examples will be found in the future.

Finally, new ^{16}Ne excited states with total decay energy of $E'_T = 5.21(10)$ and 7.60(20) MeV [corresponding $E^* = 8.37(10)$ and 10.76(20) MeV] were observed in the ^{13}N+p+p+p exit channel. There is some evidence that both these peaks have a sequential component in their decay dynamics with intermediate populations of the $E^* = 6.59$ MeV, $J^\pi = 2^+$ resonance in ^{14}O.

Acknowledgments — This material is based upon work supported by the U.S. Department of Energy, Office of Science, Office of Nuclear Physics under Award numbers DE-FG02-87ER-40316 and DE-FG02-04ER41320 and the National Science Foundation under grants PHY-1102511 and PHY-9977707. L.V.G. is partly supported by the Russian Foundation for Basic Research grant No. 14-02-00090 and the Russian Ministry of Education and Science grant No. NSh-932.2014.2. K.W.B. is supported by the National Science Foundation Graduate Research Fellowship under grant No. DGE-1143954.

[1] M. Pfützner, M. Karny, L. V. Grigorenko, and K. Riisager, Rev. Mod. Phys. **84**, 567 (2012).
[2] K. W. Brown, R. J. Charity, L. G. Sobotka, Z. Chajecki, L. V. Grigorenko, I. A. Egorova, Y. L. Parfenova, M. V. Zhukov, S. Bedoor, W. W. Buhro, J. M. Elson, W. G. Lynch, J. Manfredi, D. G. McNeel, W. Reviol, R. Shane, R. H. Showalter, M. B. Tsang, J. R. Winkelbauer, and A. H. Wuosmaa, Phys. Rev. Lett. **113**, 232501 (2014).
[3] V. I. Goldansky, Nucl. Phys. **19**, 482 (1960).
[4] I. A. Egorova, R. J. Charity, L. V. Grigorenko, Z. Chajecki, D. Coupland, J. M. Elson, T. K. Ghosh, M. E. Howard, H. Iwasaki, M. Kilburn, J. Lee, W. G. Lynch, J. Manfredi, S. T. Marley, A. Sanetullaev, R. Shane, D. V. Shetty, L. G. Sobotka, M. B. Tsang, J. Winkelbauer, A. H. Wuosmaa, M. Youngs, and M. V. Zhukov, Phys. Rev. Lett. **109**, 202502 (2012).
[5] L. V. Grigorenko, I. A. Egorova, R. J. Charity, and M. V. Zhukov, Phys. Rev. C **86**, 061602 (2012).
[6] I. Mukha, K. Sümmerer, L. Acosta, M. A. G. Alvarez, E. Casarejos, A. Chatillon, D. Cortina-Gil, I. A. Egorova, J. M. Espino, A. Fomichev, J. E. García-Ramos, H. Geissel, J. Gómez-Camacho, L. Grigorenko, J. Hofmann, O. Kiselev, A. Korsheninnikov, N. Kurz, Y. A. Litvinov, E. Litvinova, I. Martel, C. Nociforo, W. Ott, M. Pfützner, C. Rodríguez-Tajes, E. Roeckl, M. Stanoiu, N. K. Timofeyuk, H. Weick, and P. J. Woods, Phys. Rev. C **82**, 054315 (2010).
[7] F. Wamers, J. Marganiec, F. Aksouh, Y. Aksyutina, H. Álvarez-Pol, T. Aumann, S. Beceiro-Novo, K. Boretzky, M. J. G. Borge, M. Chartier, A. Chatillon, L. V. Chulkov, D. Cortina-Gil, H. Emling, O. Ershova, L. M. Fraile, H. O. U. Fynbo, D. Galaviz, H. Geissel, M. Heil, D. H. H. Hoffmann, H. T. Johansson, B. Jonson, C. Karagiannis, O. A. Kiselev, J. V. Kratz, R. Kulessa, N. Kurz, C. Langer, M. Lantz, T. Le Bleis, R. Lemmon, Y. A. Litvinov, K. Mahata, C. Müntz, T. Nilsson, C. Nociforo, G. Nyman, W. Ott, V. Panin, S. Paschalis, A. Perea, R. Plag, R. Reifarth, A. Richter, C. Rodriguez-Tajes, D. Rossi, K. Riisager, D. Savran, G. Schrieder, H. Simon, J. Stroth, K. Sümmerer, O. Tengblad, H. Weick, C. Wimmer, and M. V. Zhukov, Phys. Rev. Lett. **112**, 132502 (2014).
[8] K. Föhl, R. Bilger, H. Clement, J. Gräter, R. Meier, J. Pätzold, D. Schapler, G. J. Wagner, O. Wilhelm, W. Kluge, R. Wieser, M. Schepkin, R. Abela, F. Foroughi, and D. Renker, Phys. Rev. Lett. **79**, 3849 (1997).
[9] L. V. Grigorenko, T. D. Wiser, K. Mercurio, R. J. Charity, R. Shane, L. G. Sobotka, J. M. Elson, A. H. Wuosmaa, A. Banu, M. McCleskey, L. Trache, R. E. Tribble, and M. V. Zhukov, Phys. Rev. C **80**, 034602 (2009).
[10] L. V. Grigorenko and M. V. Zhukov, Phys. Rev. C **76**, 014008 (2007).
[11] L. V. Grigorenko and M. V. Zhukov, Phys. Rev. C **76**, 014009 (2007).
[12] L. V. Grigorenko, I. G. Mukha, I. J. Thompson, and M. V. Zhukov, Phys. Rev. Lett. **88**, 042502 (2002).
[13] L. V. Grigorenko, T. A. Golubkova, and M. V. Zhukov, Phys. Rev. C **91**, 024325 (2015).
[14] M. Wallace, M. Famiano, M.-J. van Goethem, A. Rogers, W. Lynch, J. Clifford, F. Delaunay, J. Lee, S. Labostov, M. Mocko, L. Morris, A. Moroni, B. Nett, D. Oostdyk, R. Krishnasamy, M. Tsang, R. de Souza, S. Hudan, L. Sobotka, R. Charity, J. Elson, and G. Engel, Nuclear Instruments and Methods in Physics Research Section A: Accelerators, Spectrometers, Detectors and Associated Equipment **583**, 302 (2007).
[15] A. H. Wuosmaa, B. B. Back, S. Baker, B. A. Brown, C. M. Deibel, P. Fallon, C. R. Hoffman, B. P. Kay, H. Y.

Lee, J. C. Lighthall, A. O. Macchiavelli, S. T. Marley, R. C. Pardo, K. E. Rehm, J. P. Schiffer, D. V. Shetty, and M. Wiedeking, Phys. Rev. Lett. **105**, 132501 (2010).
[16] L. V. Grigorenko, Y. L. Parfenova, and M. V. Zhukov, Phys. Rev. C **71**, 051604 (2005).
[17] K. Ogawa, H. Nakada, S. Hino, and R. Motegi, Physics Letters B **464**, 157 (1999).
[18] H. T. Fortune, Phys. Rev. C **74**, 054310 (2006).
[19] G. J. KeKelis, M. S. Zisman, D. K. Scott, R. Jahn, D. J. Vieira, J. Cerny, and F. Ajzenberg-Selove, Phys. Rev. C **17**, 1929 (1978).
[20] J. Marganiec, F. Wamers, F. Aksouh, Y. Aksyutina, H. Álvarez-Pol, T. Aumann, S. Beceiro-Novo, K. Boretzky, M. J. G. Borge, M. Chartier, A. Chatillon, L. V. Chulkov, D. Cortina-Gil, H. Emling, O. Ershova, L. M. Fraile, H. O. U. Fynbo, D. Galaviz, H. Geissel, M. Heil, D. H. H. Hoffmann, H. T. Johansson, B. Jonson, C. Karagiannis, O. A. Kiselev, J. V. Kratz, R. Kulessa, N. Kurz, C. Langer, M. Lantz, T. Le Bleis, R. Lemmon, Y. A. Litvinov, K. Mahata, C. Müntz, T. Nilsson, C. Nociforo, G. Nyman, W. Ott, V. Panin, S. Paschalis, A. Perea, R. Plag, R. Reifarth, A. Richter, C. Rodriguez-Tajes, D. Rossi, K. Riisager, D. Savran, G. Schrieder, H. Simon, J. Stroth, K. Sümmerer, O. Tengblad, H. Weick, C. Wimmer, and M. V. Zhukov, Eur. Phys. J. A **51**, 9 (2015).